X-wave solutions of complex Ginzburg-Landau equations

C. T. Zhou,[1] M. Y. Yu,[2] and X. T. He[1]
[1]*Institute of Applied Physics and Computational Mathematics, P.O. Box 8009, Beijing 100088, People's Republic of China*
[2]*Institut für Theoretische Physik I, Ruhr-Universität Bochum, D-44780 Bochum, Germany*
(Received 29 August 2005; published 14 February 2006; corrected 22 February 2006)

A solution in the form of X-wave patterns of the complex Ginzburg-Landau equation with a harmonic background inhomogeneity is obtained. The pattern can be attributed to the effects of the harmonic potential and the boundary configuration and size. By varying the harmonic of the background potential, the competition among three types of wave patterns: spiral, X, and target, is investigated by following the evolution of the Fourier modes.

DOI: 10.1103/PhysRevE.73.026209 PACS number(s): 89.75.Kd, 05.45.Jn, 05.45.Yv, 82.40.Np

I. INTRODUCTION

Spiral and target wave patterns have often been observed in reaction-diffusion systems such as the Belousov-Zhabotinsky chemical reaction [1,2]. They have also been found in biological systems such as the cardiac muscle tissue and slime mold colonies of *Dictyostelium* [3], as well as physical systems such as the planar dc semiconductor-gas discharge [4] and large-aspect-ratio lasers [5]. Spiral and target waves are usually investigated theoretically by means of the complex Ginzburg-Landau equation (CGLE), which is a universal model for describing the evolution of nearly coherent waves. Depending on the problem involved, it can appear in various forms involving complex coefficients and nonlinearities [6–9]. The CGLE has been extensively applied to different physical, chemical, and biological systems, such as transversely extended laser, electrohydrodynamic convection in liquid crystal, Bose-Einstein condensate, fluid and chemical turbulence, planar gas discharge, plasma surface-wave oscillation, bluff body motion, etc. [1–12], and is closely related to the nonlinear Schrödinger [13,14] or Gross-Pitaevsky equation. Waves as well as pattern solutions of various forms and limits of the CGLE have been theoretically investigated by several authors [4,15–17], and it has been found that the actual solution, in particular, the target pattern, strongly depends on the medium inhomogeneity and the boundary condition.

Existing results indicate that singly charged spiral solutions of the two-dimensional (2D) CGLE are dynamically stable in some parameter regimes [9], but spirals with zero topological charge are always unstable. Target waves arising from boundary effects have also been observed [15]. By introducing localized inhomogeneity in the CGLE, Hendrey and co-workers [16,17] found that stationary and breathing target waves can also occur. Stationary target patterns have been observed in the light-sensitive Belousov-Zhabotinsky reaction [18].

On the other hand, X- or cross-shaped wave patterns have also been observed in various physical systems. They are well known in the context of linear propagation of acoustic and electromagnetic waves [19–23]. By using beam-shaping techniques, one can also obtain X waves in optical [24] and microwave radiation [25]. Recently, in connection with self-trapped optical wave packets the investigation of X waves has been extended to the nonlinear regime [26–28]. X waves can be spontaneously generated because of nonlinearities in the source or medium through wave-matter interaction. They have been found to be rather robust and can propagate or survive for long times or distances. Such waves can thus be expected in many fields. In this paper, we show numerically that if the medium is quadratic, or harmonic, the CGLE can admit X-wave solutions. The formation and stability behavior of the latter are explored. It is found that the X-shaped patterns depend on the harmonic number of the inhomogeneity as well as the boundary condition, and that they are robust.

The paper is organized as follows: In Sec. II, the problem is formulated. In Sec. III, we numerically investigate the generation of spiral-, X-, and target-wave patterns. In Sec. IV, the competition among the three types of wave patterns is analyzed. The formation of X waves is investigated in terms of the system size and the background inhomogeneity. In Sec. V, the effects of the boundary shape and type as well as the stability of the X wave is studied. The results are summarized and discussed in the final section.

II. FORMULATION

The 2D CGLE of interest here is given by

$$\partial_t \Psi = \mu(\mathbf{x})\Psi + (1+i\alpha)\nabla_\perp^2 \Psi - (1+i\beta)|\Psi|^2\Psi, \qquad (1)$$

where $\Psi(x,y,t)$ is a complex function of time t and space $\mathbf{x}$, and $\nabla_\perp^2 = \partial_x^2 + \partial_y^2$. Equation (1) is a universal model for many phenomena near the threshold of a long-wavelength oscillatory instability. In Eq. (1), $\mu(\mathbf{x})$ characterizes the property of the medium and gives the linear frequency and/or the growth and/or damping rate of the normal oscillations, the second term corresponds to spatial diffusion (real part) and dissipation (imaginary part), and the last term corresponds to the nonlinear effects (with an imaginary part describing the nonlinear frequency shift). In the limit $(\alpha,\beta)\to\infty$, Eq. (1) reduces to the widely investigated cubic nonlinear Schrödinger or Gross-Pitaevsky equation. Depending on the parameters α and β, defect or phase turbulence of the complex quantity Ψ may occur, resulting in spatiotemporal

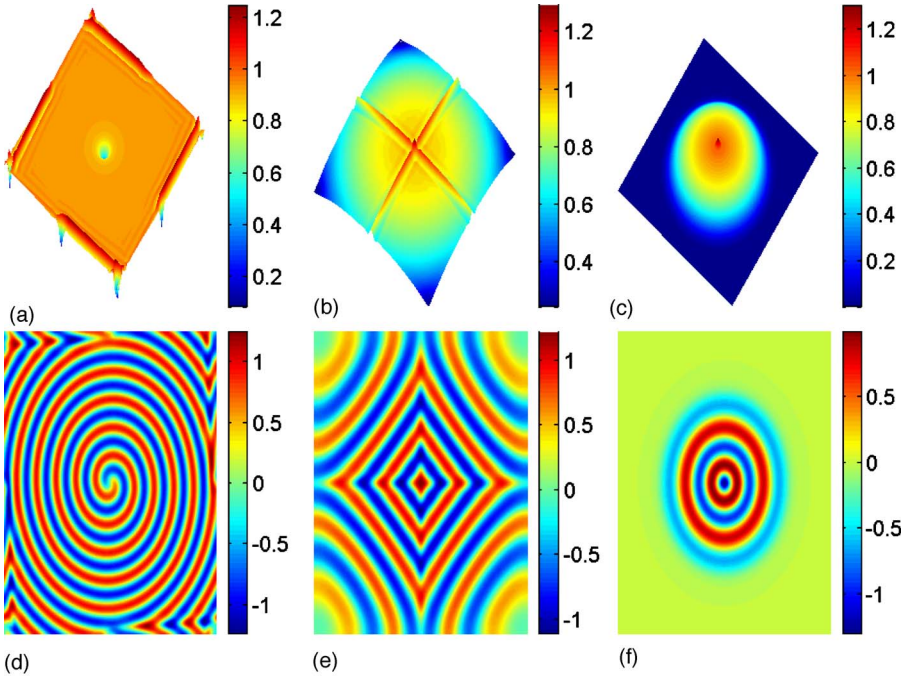

FIG. 1. (Color online) Examples of the three stationary wave patterns at $t=200$. The labels (a), (b), and (c) correspond to three subplots of the first row (from the left to right) and (d), (e), and (f) correspond to three subplots of the second row. (a), (b), and (c) give the amplitude $|\Psi(x,y,t)|$ and (d), (e), and (f) give the corresponding real part $\mathrm{Re}\,\Psi(x,y,t)$. The parameters of the CGLE are $[\alpha,\beta]=[3.5,-0.34]$, and the size of the system is $L=200\times200$. The corresponding external frequencies are $\Omega=0$ in (a) and (d), $\Omega=0.01$ in (b) and (e), and $\Omega=0.02$ in (c) and (f).

chaotic solitons [9,29].

In the limit $\mu=1$, analysis of the local bifurcation properties indicates that the plane-wave solution [29], $\Psi=\sqrt{1-k^2}e^{i(\mathbf{k}\cdot\mathbf{x}-\omega t)}$ with $|k|\leqslant1$ and frequency $\omega=\beta+(\alpha-\beta)k^2$, is linearly stable in the range $|k|\leqslant k_c$ with $k_c=\sqrt{(1+\alpha\beta)/(3+\alpha\beta+2\beta^2)}$. The stability range vanishes at the Benjamin-Feir-Newell line $\alpha\beta=-1$, and no stable plane-wave solution exists for $\alpha\beta<-1$. For a wide range of α and β, the 2D CGLE (1) possesses rotating spiral solutions in the form [30]

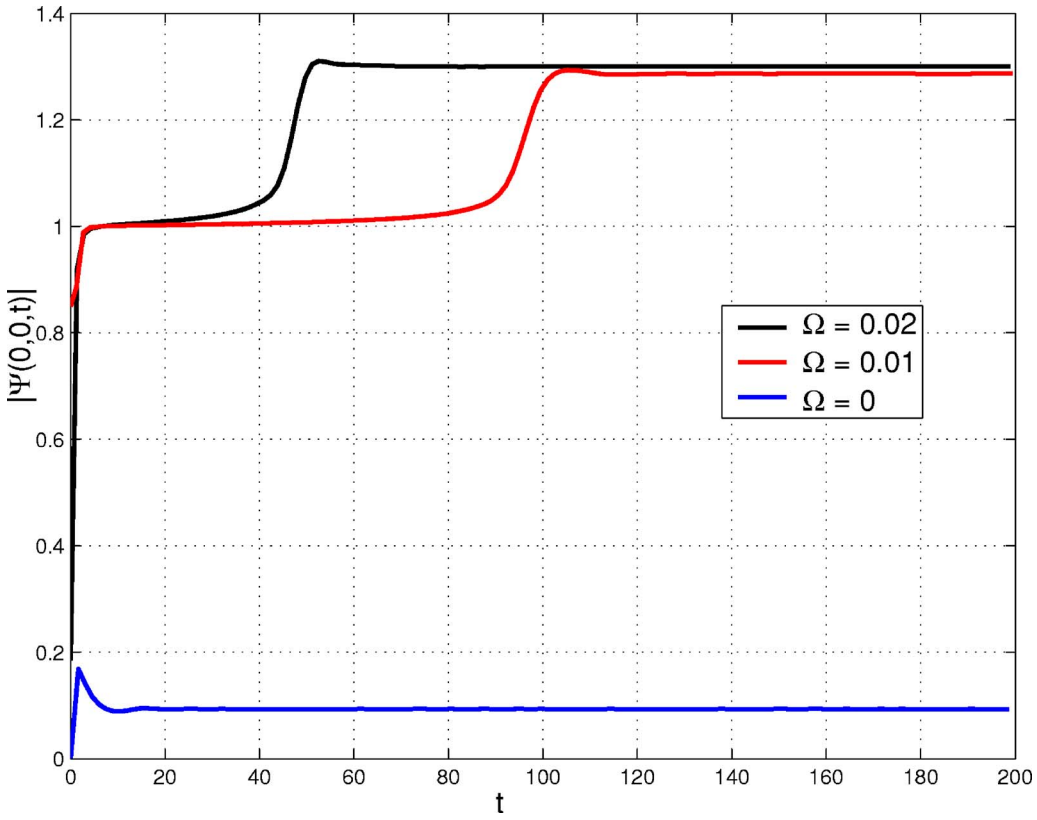

FIG. 2. (Color online) The evolution of the amplitude $|\Psi(0,0,t)|$ at the center of the simulated system for $\Omega=0$, 0.01, and 0.02, corresponding to the spiral, X, and target patterns, respectively.

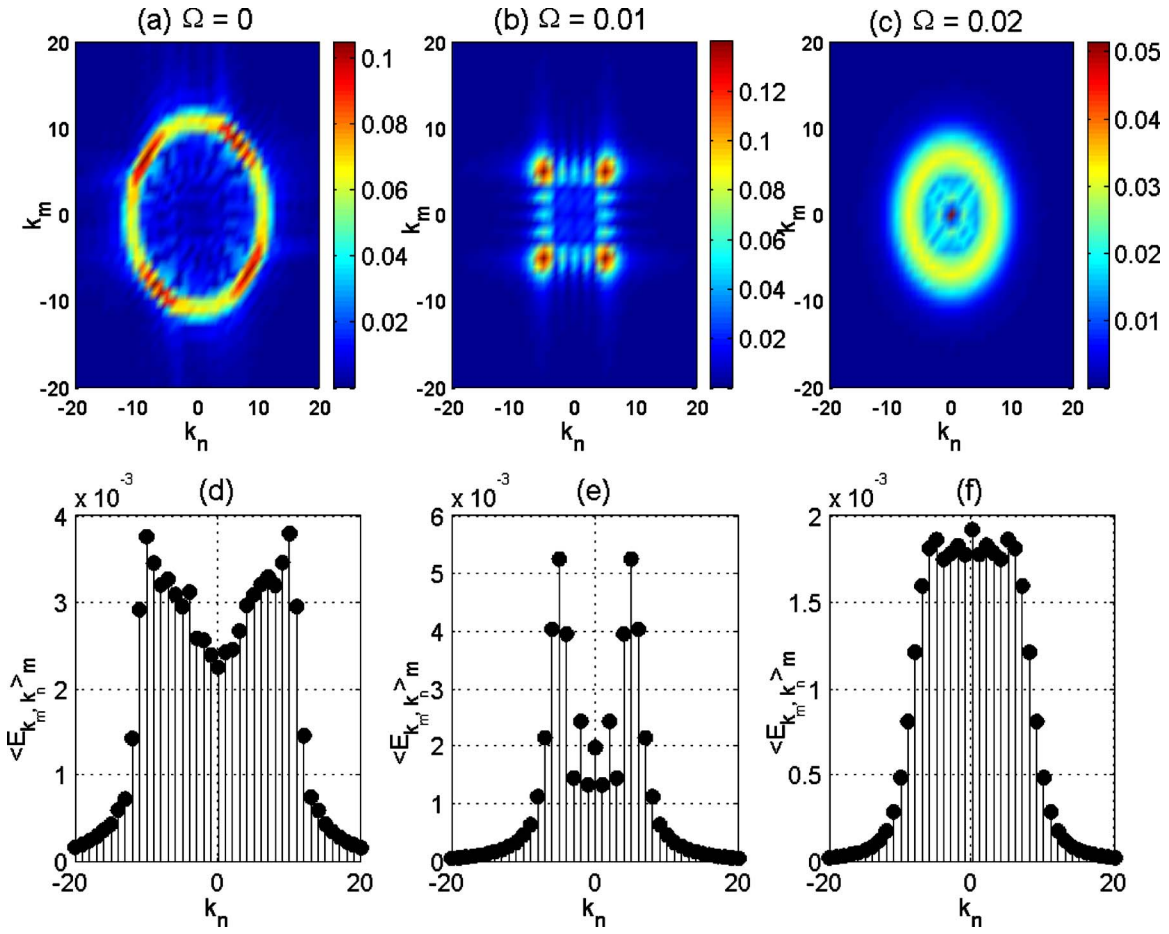

FIG. 3. (Color online) Spectral structures corresponding to Fig. 1. (a), (b), and (c) give the spectral amplitude $|\Psi(k_m,k_n,t)|$ and (d), (e), and (f) give the average spectrum $\langle|\Psi(k_m,k_n,t)|\rangle_m$. The external frequencies are (a) and (d): $\Omega=0$, (b) and (e): $\Omega=0.01$, and (c) and (f): $\Omega=0.02$, corresponding to the spiral, X, and target patterns, respectively.

$$\Psi(r,\theta,t) = F(r)e^{i[-\omega t+m\theta+\phi(r)]}$$

with $\Psi=0$ at the spiral core. For a target wave (i.e., when $\theta=0$), concentric oscillations propagate from an oscillatory centrum.

In many physical applications of the CGLE, the medium is inhomogeneous, or $\mu=\mu(\mathbf{x})$. In this case stable superspiral [31] as well as target waves can appear if there is exponential spatial dependence in both the real and imaginary parts of $\mu(r)$ [16,17]. It has been found that the lowest-order effect of the inhomogeneity is a strong dependence of the local frequency and growth rate of the excitation in space [16,17]. Here we shall use the often-invoked harmonic- or quadratic-potential model [7,8] for the inhomogeneity: $\mu(r)=1-\frac{1}{2}\Omega^2r^2$. Physically, this dependence approximates the bottom of any trapping potential. It allows trapping of waves or particles in a simple potential well, and the corresponding Einstein frequency is Ω [32]. Such a potential has often been associated with classical systems describing crystal structure, as well as with the more recent vortex-dynamics systems such as that related to Bose-Einstein condensates [33–36]. It is also used in more practical systems such as optical-fiber and plasma guides and traps [7,8]. The potential can appear naturally (as in crystals), manufactured (as in optical fibers), or externally introduced (such as by electric and magnetic fields in plasmas and rotation in fluids), or by other means (such as by shining laser light on the light-sensitive Belousov-Zhabotinsky reaction [18]).

By means of numerical experiments, we look for wave-pattern solutions of Eq. (1) for different Ω. For definiteness, we shall assume $\alpha=3.5$ and $\beta=-0.34$, that are typical for studying spiral waves [29]. The numerical solution is performed using fast Fourier transform for the space variables x and y, and a variable-step fourth-order Runge-Kutta scheme for the time variable. Such a periodic boundary condition approach is applicable to many physical systems and is frequently used in numerical simulations. Unless otherwise stated, the system size is $L=200\times200$, and the number of Fourier modes is taken to be between $2^7\times2^7$ and $2^9\times2^9$. As an initial condition, in order not to favor any particular type of solution, we use a random distribution of small-amplitude fluctuations. For $\Omega=0$, it is found that *any* initial condition consisting of small-amplitude waves with a topological charge will rapidly evolve into spiral waves.

III. SPIRAL-, X-, AND TARGET WAVES

Three types of wave patterns corresponding to $\Omega=0$, 0.01, and 0.02 are shown in Figs. 1(a)–1(c), respectively. The

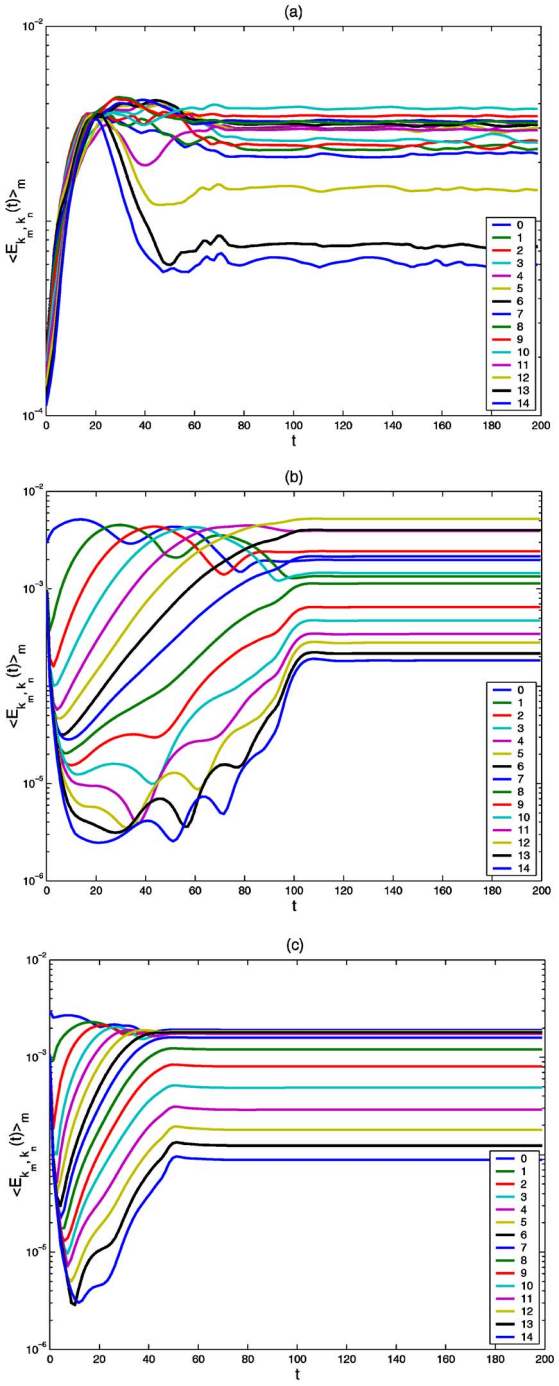

FIG. 4. (Color online) Evolution of the first 15 averaged spectral amplitudes (inset) $\langle|\Psi(k_m,k_n,t)|\rangle_m$ (for $n=0,\ldots,14$) for (a) $\Omega=0$, (b) $\Omega=0.01$, and (c) $\Omega=0.02$, corresponding to the spiral, X, and target patterns, respectively. The very distinct evolution characteristics (see text) of the three wave patterns can be observed.

snapshots are taken at $t=200$. The upper row shows $|\Psi(x,y,t)|$ and the lower row shows $\mathrm{Re}\,\Psi(x,y,t)$. Figure 1(a) shows that when $\Omega=0$, the amplitude represents a point source in a spiral core, corresponding to a typical spiral pattern for the real part Re Ψ, given in Fig. 1(d), of the complex field $\Psi(x,y,t)$. Recall that the real part and the phase of the latter are, in general, of the same topological structure. The case $\Omega=0.02$ corresponds to the stationary target-wave pattern and has been investigated for homogeneous as well as inhomogeneous CGLE [16,17]. The spirals rotate in time at the Hopf frequency ω given by the imaginary part of the eigenvalue found in the linear analysis. The homogeneous case yields spirals with the same frequency ω. The spiral centers can be identified by the dark spots in the amplitude plot given by Fig. 1(a) or as the center of the spiral waves in the Re Ψ phase plot, given by Fig. 1(d). However, when the homogeneity is destroyed by an external harmonic potential, the wave energy propagates from the outer domain to the center within a short time, leading to the disappearance of the point singularity at the center of the spiral waves. As long as Ω is sufficiently larger than the characteristic oscillation frequency ω of the system, most of the energy is concentrated in the center region of the system and the phase becomes concentric oscillations propagating from an oscillatory centrum. When the equilibrium corresponding to these two frequencies is reached before the waves from the center can arrive at the boundary, one easily gets a stationary target-wave pattern. The corresponding patterns of $|\Psi|$ and Re Ψ are shown in Figs. 1(c) and 1(f).

However, if the interaction of the outward wave with the boundary occurs before equilibrium is reached, the boundary effect would lead to a new spatially local wave pattern, whose amplitude maxima are at the centers of the four boundary walls. The role of the real part [Fig. 1(d)] of the complex field (or the phase) is enhanced by the boundary effect. The balance between dispersion and trapping by the harmonic background potential as well as the walls results in an interesting X-wave structure, as shown in Fig. 1(b). It is found that the very-well-defined coherent X pattern can occur in the parameter regime $\Omega\in[0.005,0.015]$. Unlike the spiral waves, the existence of X waves depends sensitively on the size of the system (with fixed Ω), a property which will be further discussed below. Finally, it is worth noting that the three wave patterns in Figs. 1(d)–1(f) are of similar topological structure as that of low-dimensional phase trajectories (with respect to the node-, saddle- and center-point behavior) in dynamical systems. This similarity leads to the still unanswered question of whether there is topological relationship between low- and infinite-dimensional systems, a problem that is beyond the scope of the present work.

To see how the external harmonic potential affects the formation of the wave patterns, we have also analyzed the time evolution of the wave amplitude at the system center. Figure 2 shows that the defect in the spiral waves can occur in the presence of the external potential. An initial core with low energy can absorb traveling waves and rapidly become a high-energy center because of the harmonic potential. On the other hand, dispersion can cause an outflow of wave energy. A stationary state occurs when a balance among dispersion and/or dissipation, harmonic-potential trapping, and nonlinear effects is reached. Figure 2 shows that with different Ω values, stationary wave patterns are eventually formed, and the time needed to reach the asymptotic stationary state becomes shorter with increasing Ω. We note that the formation of the X wave is associated with a long $(5\leqslant t\leqslant 110)$ evolution time, while the target wave reaches its final stationary state already at $t\sim 50$.

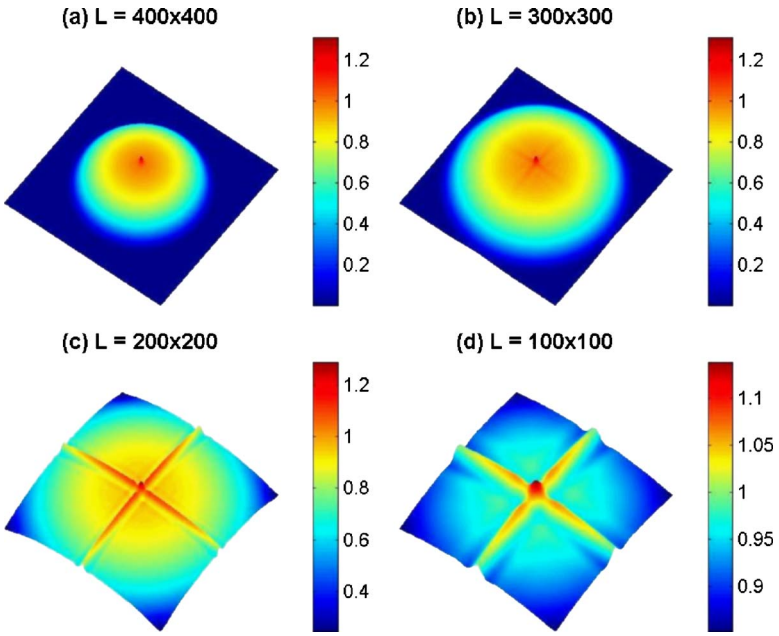

FIG. 5. (Color online) Dependence of the amplitude $|\Psi(x,y,t=200)|$ on the size of the system. (a) $L=400\times400$, (b) $L=300\times300$, (c) $L=200\times200$, and (d) $L=100\times100$. The other parameters are the same as in Fig. 1.

IV. FORMATION OF X WAVES

In order to better understand the X waves, it is useful to analyze the energy distribution associated with the coherent patterns and their formation. The 2D Fourier spectrum $|\Psi(k_m,k_n)|$, where k_m and k_n are the wave numbers in the x and y directions, are given in Fig. 3. The parameters are the same as that for Fig. 1. One can see that each wave pattern has a distinct spectral distribution. For the spiral wave [Fig. 3(a)], much of the energy is nonuniformly distributed in a ring structure and there is a dip at $\mathbf{k}=\mathbf{0}$. For the X wave [Fig. 3(b)], the energy is distributed in the form of concentrate squares, with the energy maxima in each square at the four corners. The absence of the isotropic ring structure here implies a dominance of the wall effects. For the target wave [Fig. 3(c)], we again have an isotropic, but now table-top structure. Since the energy spectra for the three patterns exhibit x,y symmetry, for analyzing the energy distribution more quantitatively one can take the mode average over one of the two wave-number spaces. In Figs. 3(d)–3(f), we show $\langle|\Psi(k_m,k_n,t)|\rangle_m$, where $\langle\cdots\rangle_m$ indicates that the average has been taken over the Fourier modes in the x direction. For the spiral wave [Figs. 3(a) and 3(d)], the spectrum is peaked at $k_n=\pm10$ and its decrease as $|k_n|\to0$ is almost monotonic. For the X wave [Figs. 3(b) and 3(e)], the spectrum is sharply

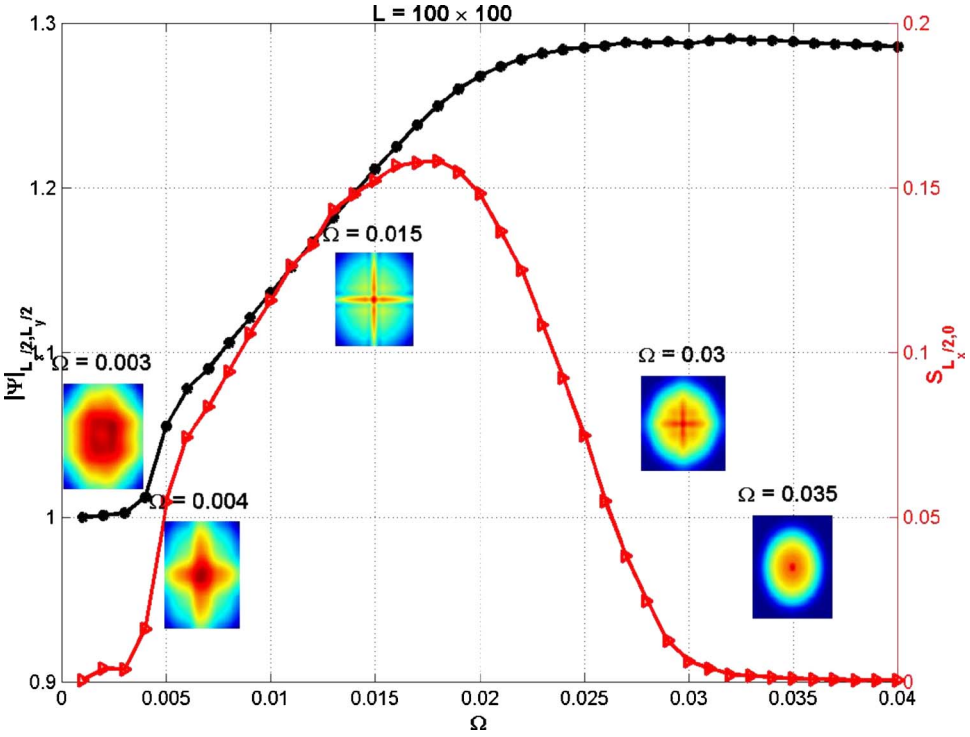

FIG. 6. (Color online) Dependence of the amplitude at the system center (triangles) and the boundary point $(L_x/2,0)$ (circles) on Ω at $t=200$ for $L=100\times100$, $\alpha=3.5$, and $\beta=-0.34$. The transition from the X to the target pattern as Ω increases can be seen from the insets.

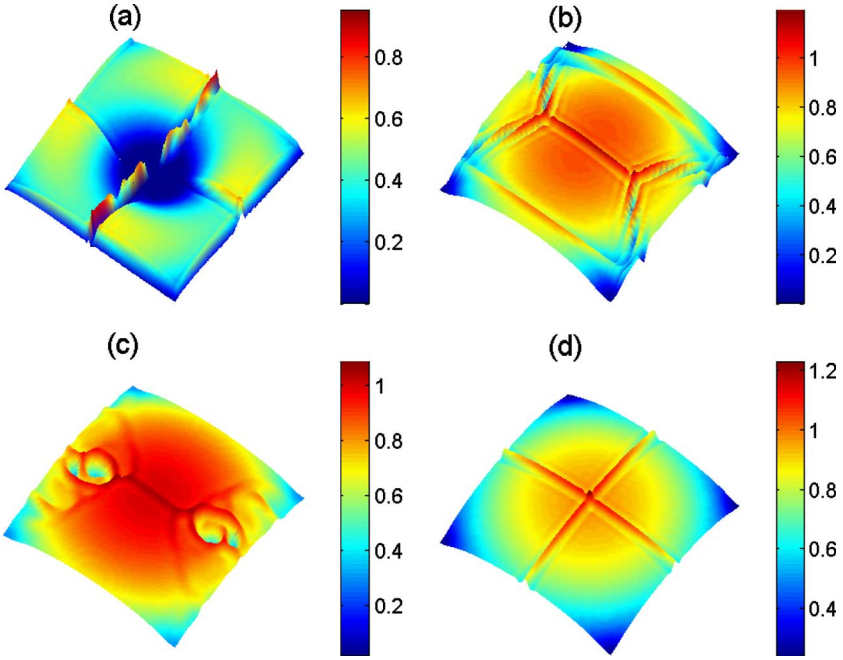

FIG. 7. (Color online) Evolution of a perturbed X pattern. The field at $t=200$ in Fig. 1(b) is perturbed by adding a phase $e^{im\theta}$ (with charge $m=3$) in the period $t=200-205$. (a), (b), and (c) show the transient states of the amplitude $|\Psi(x,y,t)|$ at $t=201.109$, 227.641, and 302.503. (d) shows the final asymptotic or stationary state.

peaked at the two modes $k_n=\pm 5$, and the energy decrease as $|k_n|\to 0$ is in an oscillatory manner. Most of the energy is in the modes $k_n=\pm 5$ and their neighbors $k_n=\pm 4, \pm 6$. For the target waves [Figs. 3(a) and 3(d)], on the other hand, most of the energy is evenly distributed among the first 13 modes $k_n=0, \pm 1, \ldots, \pm 6$.

In the formation process of the coherent patterns, energy exchange or cascade among the different Fourier modes plays an important role. To investigate this, we follow the evolution of the average energy of the first 50 modes starting from the initial random state. The results are given in Fig. 4. Distinct evolution behavior of the three patterns can be observed. To which pattern the system eventually evolves depends on how energy is partitioned. For the spiral wave, the nonlinear mode-mode interaction is quite complicated. Figure 4(a) shows that an energy exchange among the modes between $k_n=1$ and $k_n=9$ always occurs for $t>50$. Thus, the spiral-wave solution found here appears to be a stationary solution of the 2D CGLE. Figures 4(b) and 4(c) show that for both the X and target waves, no mode-mode energy exchange takes place after a certain time, indicating that these patterns are stationary or quasistationary. The times needed to form stationary coherent states are approximately 110 and 50 for the X and target waves, respectively. Moreover, the energy cascade or self-organization process in the Fourier space for these two patterns is completely different. For tar-

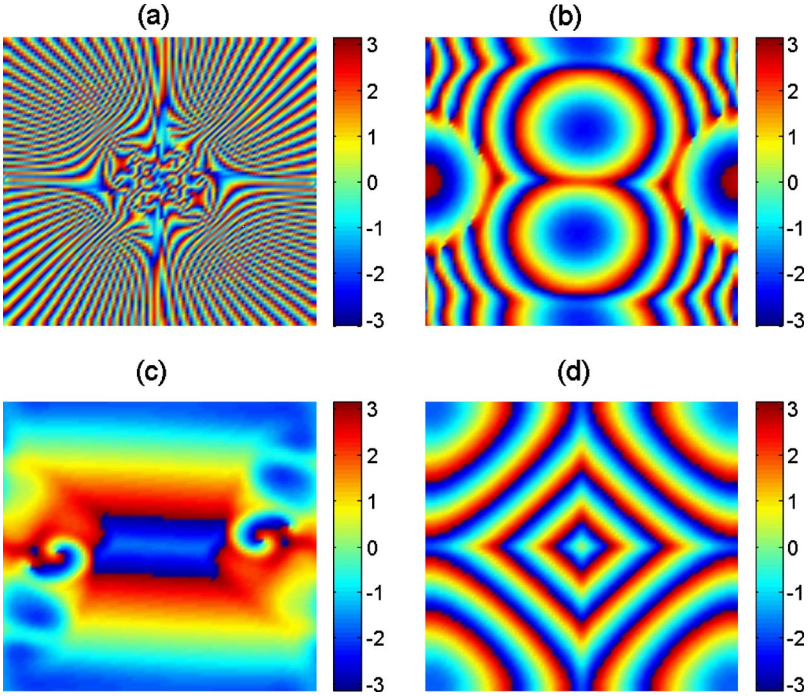

FIG. 8. (Color online) The phase $[\mathrm{Im}\,\Psi(x,y,t)]$ states corresponding to the evolution of the perturbation in Fig. 7. The phase scale is in arbitrary units.

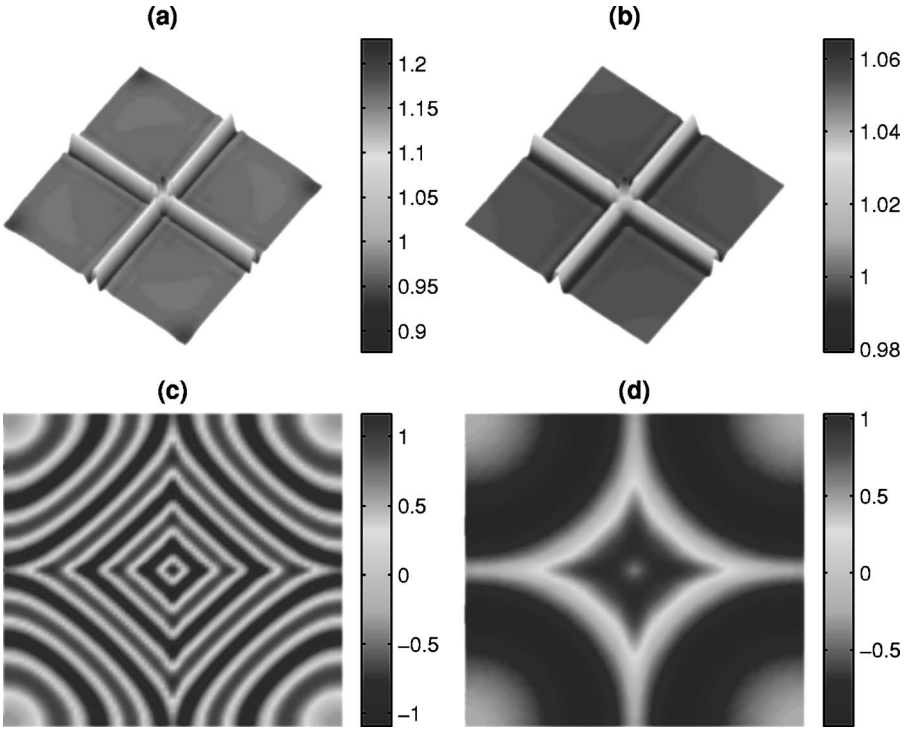

FIG. 9. Evolution of the X wave appearing in 1(b) with the inhomogeneity turned off (Ω set to zero) at $t=200$. (a) and (c) show the amplitude ($|\Psi(x,y,t)|$) and phase [$\mathrm{Im}\,\Psi(x,y,t)$] of the transient state at $t=202.48$, respectively. (b) and (d) show the same parameters for the asymptotic state at $t=400$.

get waves, the energy in the higher-order modes ($k_n>7$) is first partitioned, then the energy among the low-order modes ($k=0,\ldots,7$) is reorganized during $20\leqslant t\leqslant 50$ until the process stops. Figure 4(b) shows that for the X wave there exist two independently interacting groups of modes. The two groups are separated by the modes $k_n=8,9,10$, that do not exchange their energy among themselves nor with the other modes. On the other hand, during $20\leqslant t\leqslant 110$ strong energy exchange is observed in each of the two ($0\leqslant k_n\leqslant 7$ and $11\leqslant k_n\leqslant 14$) interacting groups. Thus, the formation of the patterns can be distinguished by the energy partition process among the Fourier modes.

Having discussed the energy partition process of the three coherent wave patterns, we now consider the mechanism of forming them. The dynamics of the spiral and target waves has already been discussed in the existing literature [9,16,17]. It is believed that the formation of target waves is due to boundary [5,15] or local-inhomogeneity [16,17] effects. With the latter mechanism, Hendrey and co-workers [16,17] found that the lowest-order inhomogeneity effect is sufficient to form a target wave. On the other hand, as pointed out by Aranson *et al.* [5] in connection with a modified complex Swift-Hohenberg equation, boundary effects are important in selecting the different patterns in large-aperture lasers. They showed that traveling waves with well-defined wave numbers emitted by the boundary can collide in the interior of the domain, forming a sink with shocklike structure. It is thus of interest to see if a similar mechanism can lead to the X-shaped coherent wave pattern. To investigate boundary-driven selection processes for the different patterns, we fix $\Omega=0.01$ and vary the size of the system. As shown in Fig. 1(b), the parameter values $\Omega=0.01$ and $L=200\times 200$ result in an X wave. In order to see the boundary dependence, we consider three cases: $L=400\times 400$, 300×300, and 100×100. Figure 5 shows the amplitude of $\Psi(x,y,t=200)$ for different system sizes. Figure 5(a) indicates that for a large system the final asymptotic state is a target pattern. In Fig. 5(b), where $L=300\times 300$, one can see that a weak X wave is seeded within a target pattern. With decreasing system size, the X-wave pattern becomes dominant, as shown in Figs. 5(c) and 5(d). It is thus clear that, besides the external harmonic potential, size and boundary effects are important in determining if X waves can occur.

V. EFFECT OF SIZE, BOUNDARY, AND INHOMOGENEITY

To illustrate the effects of size, boundary, and the harmonic parameter Ω on the X wave, we first consider the shocklike structure at the boundary. Figure 6 shows the amplitude $|\Psi(L_x/2,L_y/2)|$ at the center of the system and the structural parameter $S_{L_y/2,0}\equiv \partial_x\Psi|_{L_y/2,0}$ for different Ω values. With increasing Ω, the amplitude becomes larger until the energy at the center saturates. Figure 6 shows that an X wave appears when $\Omega=0.004$. When $\Omega=0.018$, the X wave becomes clearly defined. When Ω is further increased, a target wave with an embedded X wave at the center starts to appear. When $\Omega\geqslant 0.035$, only the target wave remains.

The stability of the X pattern with respect to topological-charge perturbations should be considered. For convenience, we start with the X wave at $\Psi(t=200)$ as given in Fig. 1(b). To simulate the perturbation, we add topological charges to the complex field by letting $\Psi(x,y,t)=\Psi(x,y,t-\delta t)e^{im\theta}$, where the charge is $m=3$ and δt is the time step in the calculation, $\theta=\tan^{-1}(x/y)$. The perturbation persists for $t=200-205$. That is, the perturbation is represented by the azimuthal phase $e^{im\theta}$ and it is not of small amplitude. Since we have shown above that when the initial condition consists of small amplitude waves with topological charge the system

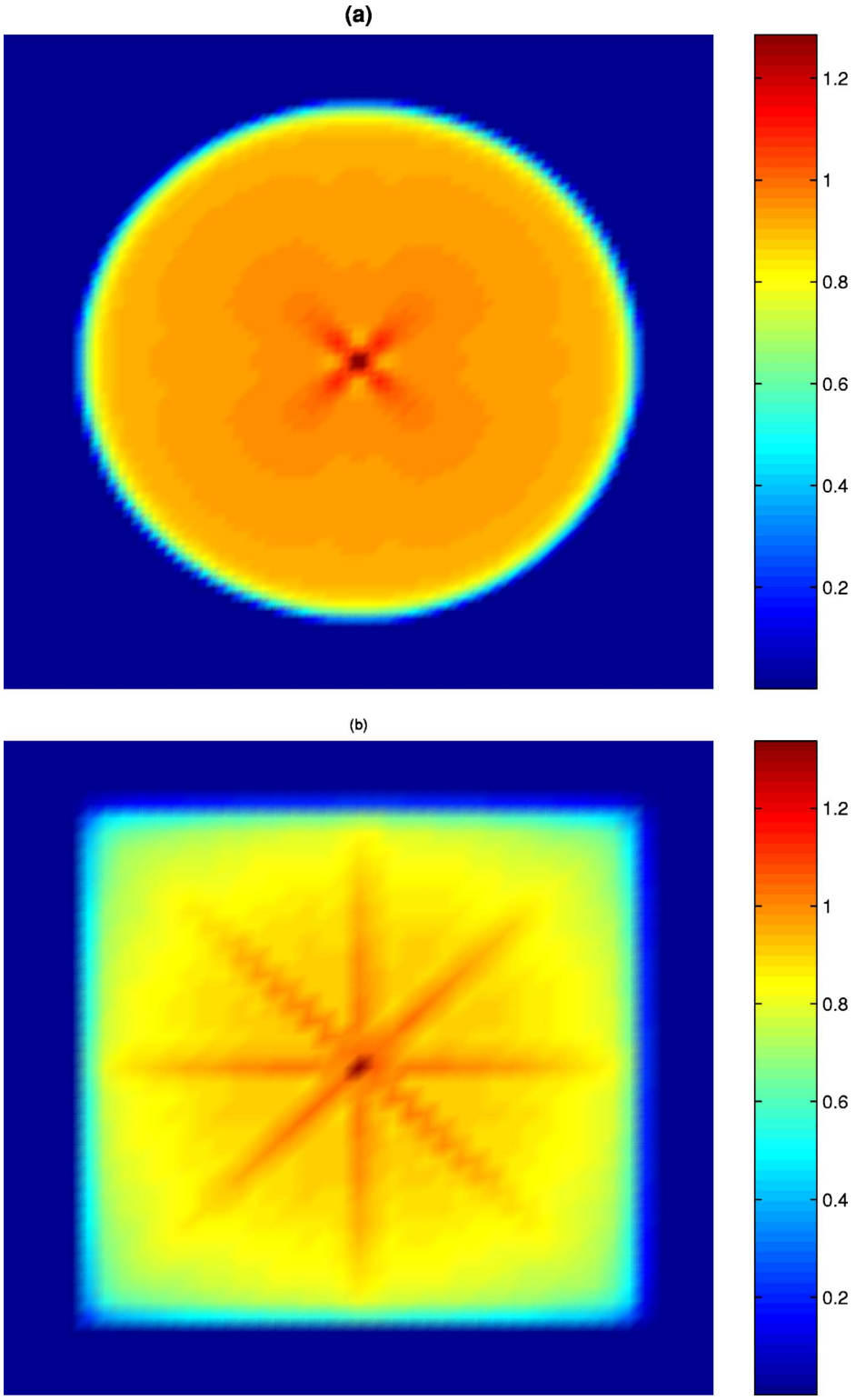

FIG. 10. (Color online) Stationary patterns for circular (a) and square (b) absorbing boundaries. The radius of the circular domain is $R=80$, and the side of the square domain is $L=160$. The parameters of the CGLE are $\alpha=3.5$, $\beta=-0.34$, and $\Omega=0.01$.

can rapidly evolve into a spiral wave, one might expect that the X pattern might be destroyed by the present topologically charged nonlinear perturbation. This turns out to be not the case. Figure 7(a) is a snapshot taken at $t=201.109$. It shows that as soon as the perturbation is introduced at $t=200$, the symmetric X pattern is rapidly disrupted. The corresponding phase, shown in Fig. 8(a), also reveals fine structuring near the system center. Later in the evolution, target-like and spiral-like patterns appear, but in a piecewise manner, as shown in Figs. 8(b) and 8(c). However, eventually the original X pattern is recovered, as shown in Figs. 7(d) and 8(d). Thus, the X wave appears to be stable to topological-charge perturbations. Since the finite-amplitude perturbed state can also be considered as a new initial state, this analysis also implies that the X wave does not depend on the initial conditions. It is only governed by the harmonic-potential param-

eter Ω, the boundary configuration, and the system size.

We have shown that with a random initial distribution of energy, the X-wave solution can only be obtained in the presence of the harmonic inhomogeneity. An unsolved question is whether the X wave can also be a stationary solution of the *homogeneous* CGLE. To answer this question, we start with the X wave at $\Psi(t=200)$ as given in Fig. 1(b), and turn off the harmonic inhomogeneity at $t=200$ by setting $\Omega=0$. In Fig. 9 we see that in the asymptotic state almost all of the energy becomes concentrated in the cross region of the system. Except at the center point, the energy is also more uniformly spread inside the cross. This behavior can be expected since in the absence of the trapping potential the background is uniform. By comparing Figs. 9(a) and 9(b), we see that the cross-wave pattern evolves very slowly, with more and more localization of energy in the cross. Comparing Figs. 9(c) and 9(d) we also note that the oscillation period becomes much longer as the asymptotic state is reached. This further indicates that the stationary X-wave solution may be associated with an intrinsic state of CGLE. However, in order to obtain such a stationary solution dynamically for a homogeneous system, appropriated initial conditions must be used.

Finally, we consider two additional types of boundaries. Figures 10(a) and 10(b) show $|\Psi(t=200)|$ for *absorbing* (in the sense that there is an infinitely deep potential well there [5]) circular and square boundaries, respectively. In Fig. 10(a), we see that although the system is azimuthally symmetric, one still finds an X wave at the center, with a fairly uniform energy distribution. However, the well-defined intense X-wave pattern in Fig. 1(b) for the periodic-boundary case is not recovered. We can better preserve (trap) the energy by increasing Ω, but then the asymptotic state becomes a target wave (not shown), trapped at the center by the strong harmonic potential. Figure 10(b) shows the stationary state for an *absorbing* square boundary. The pattern consists of a double-cross structure. In these figures the cross patterns are of much lower energy (compared with that for periodic boundary) because the energy is more uniformly spread across the domain as well as absorbed by the boundary. Thus, we can conclude that the well-defined single-X pattern appearing in Fig. 1 is dependent on the boundary as well as the harmonic potential, but for different boundary and harmonic conditions it can appear and behave quite differently.

VI. CONCLUSION

In an infinite homogeneous system, the waves form a continuum in the wave-number space. The existence of boundary and inhomogeneity severely limits the selection of wave numbers. As a result, the possible solutions necessarily depend on the boundary and inhomogeneity conditions. By varying the degree of the harmonic inhomogeneity, we have shown that, depending on the latter, three different types of wave patterns can appear as stationary solutions of the CGLE. In particular, we have shown that an inhomogeneous 2D CGLE in the presence of a simple harmonic potential admits an X-wave solution. The latter can be attributed to collision of outward traveling waves with the system boundary. Depending on the harmonics of the inhomogeneity, one can obtain spiral, target, as well as X patterns. By analyzing the energy spectra as well as by following the evolution of the nonlinear phase perturbation, we have shown that the X waves are nonspreading and quite robust, as have been observed experimentally. We have also introduced a simple method to control the formation of different coherent patterns through the background harmonic potential in the 2D CGLE.

It should be pointed out that the X waves are fundamentally different from the spiral and target waves. Their properties as well as their relation to other localized phenomena, such as solitons and oscillons, still remain to be investigated. On the other hand, since the CGLE has been invoked as a paradigm in a large number of physical, chemical, biological, and other systems [1–7,9–12,15–28], the present results on the robust nonspreading X-wave pattern indicate that the latter can occur in many different systems, and can thus underline future applications. On the other hand, the general properties and exact existence conditions of the X (or double-X) waves are still unknown, and should be of much interest for further analytical and experimental investigations.

ACKNOWLEDGMENTS

This work is supported by the National Natural Science Foundation of China (Grant No. 10575013), National Basic Research Project "Nonlinear Science in China", and SRF for ROCS, SEM.

[1] Q. Ouyang and J. M. Flesselles, Nature (London) **379**, 143 (1996).
[2] L. Q. Zhou and Q. Ouyang, Phys. Rev. Lett. **85**, 1650 (2000).
[3] K. J. Lee, E. C. Cox, and R. E. Goldstein, Phys. Rev. Lett. **76**, 1174 (1996).
[4] Y. A. Astrov, I. Müller, E. Ammelt, and H.-G. Purwins, Phys. Rev. Lett. **80**, 5341 (1998).
[5] I. Aranson, D. Hochheiser, and J. V. Moloney, Phys. Rev. A **55**, 3173 (1997).
[6] O. M. Gradov, L. Stenflo, and M. Y. Yu, Phys. Fluids B **5**, 1922 (1993).
[7] M. C. Cross and P. C. Hohenberg, Rev. Mod. Phys. **65**, 851 (1993).
[8] D. H. L. Dubin and T. M. O'Neil, Rev. Mod. Phys. **71**, 87 (1999).
[9] See, for example, I. S. Aranson and L. Kramer, Rev. Mod. Phys. **74**, 99 (2002), and the references therein.
[10] N. G. Berloff, Phys. Rev. Lett. **94**, 010403 (2005).
[11] L. Gurevich, A. S. Moskalenko, A. L. Zanin, Yu. A. Astrov, and H.-G. Purwins, Phys. Lett. A **307**, 299 (2003).
[12] L. Stenflo and M. Y. Yu, Nature (London) **384**, 224 (1996).
[13] C. T. Zhou, X. T. He, and S. G. Chen, Phys. Rev. A **46**, 2277

(1992).
[14] C. Zhou, X. T. He, and T. Cai, Phys. Rev. E **50**, 4136 (1994).
[15] V. M. Eguiluz, E. Hernandez-Garcia, and O. Piro, Int. J. Bifurcation Chaos Appl. Sci. Eng. **9**, 2209 (1999).
[16] M. Hendrey, E. Ott, and T. M. Antonsen, Phys. Rev. Lett. **82**, 859 (1999).
[17] M. Hendrey, K. Nam, P. Guzdar, and E. Ott, Phys. Rev. E **62**, 7627 (2000).
[18] V. Petrov, Q. Ouyang, G. Li, and H. L. Swinney, J. Phys. Chem. **100**, 18992 (1996).
[19] J. Lu and J. F. Greenleaf, IEEE Trans. Ultrason. Ferroelectr. Freq. Control **39**, 441 (1992).
[20] P. R. Stepanishen and J. Sun, J. Acoust. Soc. Am. **102**, 3308 (1997).
[21] P. Saari and K. Reivelt, Phys. Rev. Lett. **79**, 4135 (1997).
[22] J. Salo, J. Fagerholm, A. T. Friberg, and M. M. Salomaa, Phys. Rev. Lett. **83**, 1171 (1999).
[23] J. Salo, J. Fagerholm, A. T. Friberg, and M. M. Salomaa, Phys. Rev. E **62**, 4261 (2000).
[24] P. Saari and K. Reivelt, Phys. Rev. Lett. **79**, 4135 (1997).
[25] D. Mugnai, A. Ranfagni, and R. Ruggeri, Phys. Rev. Lett. **84**, 4830 (2000).
[26] C. Conti, S. Trillo, P. Di Trapani, G. Valiulis, A. Piskarskas, O. Jedrkiewicz, and J. Trull, Phys. Rev. Lett. **90**, 170406 (2003).
[27] P. Di Trapani, G. Valiulis, A. Piskarskas, J. Trull, C. Conti, and S. Trillo, Phys. Rev. Lett. **91**, 093904 (2003).
[28] S. Droulias, K. Hizanidis, J. Meier, and D. N. Christodoulides, Opt. Express **13**, 1827 (2005).
[29] H. Chaté, Nonlinearity **7**, 185 (1994).
[30] Here r and θ are the polar coordinates. The integer $m=0,\pm1,\ldots$, denotes the topological charge, ω is the rigid rotation frequency of spirals, $F(r)>0$ is the amplitude, $\psi(r)$ is the phase of the spiral. The target waves do not have a phase singularity at the center. A target wave can be thought of as having no topological charge, or $m=0$.
[31] L. Brusch, A. Torcini, and M. Bär, Phys. Rev. Lett. **91**, 108302 (2003).
[32] S. Ichimaru, *Statistical Plasma Physics Vol. II: Condensed Plasmas* (Addison-Wesley, Reading, Massachusetts, 1994).
[33] L. Khaykovich F. Schreck, G. Ferrari, T. Bourdel, J. Cubizolles, L. D. Carr, Y. Castin, and C. Salomon, Science **296**, 1290 (2002).
[34] G. Theocharis, D. J. Frantzeskakis, P. G. Kevrekidis, B. A. Malomed, and Y. S. Kivshar, Phys. Rev. Lett. **90**, 120403 (2003).
[35] M. Soljačić and M. Segev, Phys. Rev. Lett. **86**, 420 (2001).
[36] V. E. Zakharov and S. V. Nazarenkoc, Physica D **201**, 203 (2005).